

## Analytical Chemistry

# Intracellular Photophysics of an Osmium Complex bearing an Oligothiophene Extended Ligand

Kilian R. A. Schneider,<sup>[a, b]</sup> Avinash Chettri,<sup>[a, b]</sup> Houston D. Cole,<sup>[c]</sup> Katharina Reglinski,<sup>[a, d, e]</sup> Jannik Brückmann,<sup>[f]</sup> John A. Roque, III,<sup>[c, g]</sup> Anne Stumper,<sup>[f]</sup> Djawed Nauroozi,<sup>[f]</sup> Sylvia Schmid,<sup>[h]</sup> Christoffer B. Lagerholm,<sup>[i]</sup> Sven Rau,<sup>[f]</sup> Peter Bäuerle,<sup>[h]</sup> Christian Eggeling,<sup>[a, d, i]</sup> Colin G. Cameron,<sup>[c]</sup> Sherri A. McFarland,<sup>\*[c]</sup> and Benjamin Dietzek<sup>\*[a, b]</sup>

**Abstract:** This contribution describes the excited-state properties of an Osmium-complex when taken up into human cells. The complex **1** [Os(bpy)<sub>2</sub>(IP-4T)](PF<sub>6</sub>)<sub>2</sub> with bpy = 2,2'-bipyridine and IP-4T = 2-{5'-[3',4'-diethyl-(2,2'-bithien-5-yl)]-3,4-diethyl-2,2'-bithiophene}imidazo[4,5-f][1,10]phenanthroline) can be discussed as a candidate for photodynamic therapy in the biological red/NIR window. The complex is taken up by MCF7 cells and localizes rather homogeneously within in the cytoplasm. To detail the sub-ns photophysics of **1**, comparative transient absorption measurements were carried out in different solvents to derive a model of the photoinduced processes. Key to rationalize the excited-state relaxation is a long-lived <sup>3</sup>ILCT state associated with the oligothiophene chain. This model was then tested with the complex internalized into MCF7 cells, since the intracellular environment has long been suspected to take big influence on the excited state properties. In our study of **1** in cells, we were able to show that, though the overall model remained the same, the excited-state dynamics are affected strongly by the intracellular environment. Our study represents the first in depth correlation towards ex-vivo and in vivo ultrafast spectroscopy for a possible photodrug.

Transition-metal complexes, and in particular Ru<sup>II</sup> complexes,<sup>[1–3]</sup> are being investigated as photodrugs both in photodynamic therapy (PDT)<sup>[4–7]</sup> and photochemotherapy (PCT).<sup>[8–12]</sup> Both approaches rely on the administration of an agent with relatively low cytotoxicity in the dark, which, becomes orders of magnitude more toxic upon irradiation with light. Only PDT has been approved clinically, and its underlying mechanism of action involves the generation of cytotoxic singlet oxygen (<sup>1</sup>O<sub>2</sub>) and other reactive oxygen species (ROS).<sup>[13–15]</sup> PCT has focused on avoiding this oxygen dependence mainly through photoinduced ligand loss and subsequent covalent modification of biomolecules as an alternate mechanism.<sup>[16–25]</sup> While the Ru<sup>II</sup> systems that have been investigated for PDT and PCT absorb visible light, many cannot be activated with wavelengths in the so-called biological window (650–850 nm) that are desirable for deeper tissue penetration.

One strategy for shifting the optical window of metal complex phototherapy agents to longer wavelengths while building on successful molecular design concepts for Ru<sup>II</sup> complexes is to utilize the Os<sup>II</sup> analogues of the Ru<sup>II</sup> complexes.<sup>[26–30]</sup> In fact, Os<sup>II</sup> complexes are becoming widely appreciated as both therapeutic compounds<sup>[31–41]</sup> and cellular imaging agents.<sup>[42–47]</sup> This approach has been explored by McFarland and co-workers

[a] K. R. A. Schneider, A. Chettri, Dr. K. Reglinski, Prof. Dr. C. Eggeling, Prof. Dr. B. Dietzek  
Department Functional Interfaces (K.R.A.S., A.C., B.D.)  
Department Biophysical Imaging (K.R., C.E.)  
Leibniz Institute of Photonic Technology (IPHT) e. V.  
Albert-Einstein-Straße 9, 07745 Jena (Germany)  
E-mail: benjamin.dietzek@leibniz-ipht.de

[b] K. R. A. Schneider, A. Chettri, Prof. Dr. B. Dietzek  
Institute of Physical Chemistry and Abbe Center of Photonics  
Friedrich-Schiller-University Jena, Helmholtzweg 4, 07743 Jena (Germany)

[c] H. D. Cole, J. A. Roque, III, Dr. C. G. Cameron, Prof. Dr. S. A. McFarland  
Department of Chemistry and Biochemistry  
The University of Texas at Arlington, Arlington, TX 76019-0065 (USA)  
E-mail: sherri.mcfarland@uta.edu

[d] Dr. K. Reglinski, Prof. Dr. C. Eggeling  
Institute of Applied Optic and Biophysics, Friedrich-Schiller University Jena  
Max-Wien-Platz 1, 07743 Jena (Germany)


[e] Dr. K. Reglinski  
University Hospital Jena, Bachstraße 18, 07743 Jena (Germany)


[f] J. Brückmann, Dr. A. Stumper, Dr. D. Nauroozi, Prof. Dr. S. Rau  
Institute of Inorganic Chemistry I, Ulm University  
Albert-Einstein-Allee 11, 89081 Ulm (Germany)

[g] J. A. Roque, III  
Department of Chemistry and Biochemistry  
The University of North Carolina at Greensboro  
Greensboro, North Carolina, 27402 (USA)

[h] Dr. S. Schmid, Prof. Dr. P. Bäuerle  
Institute of Organic Chemistry II and Advanced Materials  
Ulm University, Albert-Einstein-Allee 11, 89081 Ulm (Germany)

[i] Dr. C. B. Lagerholm, Prof. Dr. C. Eggeling  
<MRC Human Immunology Unit & Wolfson Imaging Center Oxford  
Headley Way, Oxford, OX3 9DS (UK)

 Supporting information and the ORCID identification number(s) for the author(s) of this article can be found under:  
<https://doi.org/10.1002/chem.202002667>.

 © 2020 The Authors. Published by Wiley-VCH GmbH. This is an open access article under the terms of the Creative Commons Attribution License, which permits use, distribution and reproduction in any medium, provided the original work is properly cited.

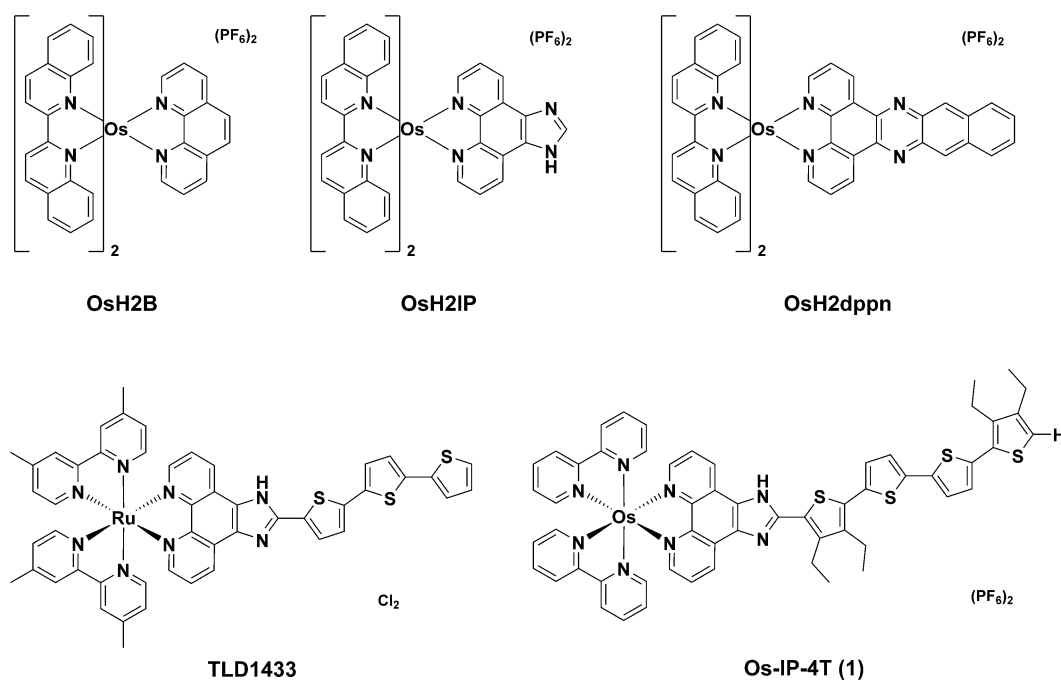
for PDT,<sup>[48]</sup> but it has not been applied to PCT given that the Os<sup>II</sup> polypyridyl counterparts are photoinert.<sup>[49,50]</sup> Both in vitro and in vivo studies of the Os<sup>II</sup> photosensitizers **OsH2B**, **OsH2IP**, and **OsH2dppn** (Scheme 1) published by McFarland and co-workers showed panchromatic activation, low dark toxicity, and PDT activity.<sup>[48,51]</sup>

Building on this work, this study details the intracellular photophysics of the novel complex **Os-IP-4T** (**1**, [Os(bpy)<sub>2</sub>(IP-4T)](PF<sub>6</sub>)<sub>2</sub> with bpy = 2,2'-bipyridine and IP-4T = 2-{5'-[3',4'-diethyl-(2,2'-bithien-5-yl)]-3,4-diethyl-2,2'-bithiophene}imidazo[4,5-f][1,10]phenanthroline), which was inspired by the Ru<sup>II</sup> complex **TLD1433** ([Ru(4,4'-dmb)<sub>2</sub>(IP-3T)]Cl<sub>2</sub> where 4,4'-dmb = 4,4'-dimethyl-2,2'-bipyridine and IP-3T = 2-(2',2''':5'',2''''-terthiophene)-imidazo[4,5-f][1,10]phenanthroline). **TLD1433** was developed by McFarland and co-workers<sup>[52-54]</sup> and is currently in Phase II human clinical studies for treating bladder cancer with PDT.<sup>[55]</sup> Our goal was to interrogate the impact of the biological target on the photophysics of the complex by studying the intracellular photophysics of **1** in MCF7 cells and comparing to the cell-free environment. We carried out a detailed cell-free photophysical study on the PF<sub>6</sub><sup>-</sup> salt of **1** in MeCN in order to be able to compare to other Os<sup>II</sup> compounds in the literature that use this salt form and solvent and to determine how the aqueous intracellular photophysical properties compare to this standard cell-free condition. The photophysical models proposed from the experimental data in this study assume predominantly one form of the potentially ionizable imidazo group of **1**.<sup>[56]</sup>

This comparative study is of particular relevance as the intracellular photophysics governs whether a compound will have photocytotoxic effects following light absorption. To truly understand the photoactivation mechanism, the light-induced

processes must not only be examined in solution but also within cancer cells. The results presented suggest a model of the excited-state dynamics involving emissive triplet metal-to-ligand charge transfer (<sup>3</sup>MLCT) states, which enable tracking of the intracellular localization of the complexes, and dark triplet intraligand charge transfer (<sup>3</sup>ILCT) states that efficiently sensitize <sup>1</sup>O<sub>2</sub>. The mechanistic work discussed herein highlights the importance of the π-extended oligothieryl-appended IP ligand in designing photoactive metal complexes with uniquely balanced <sup>3</sup>MLCT and <sup>3</sup>ILCT excited states for phototoxic effects.

The absorption spectra of **1** in the solvents dichloromethane (DCM) and acetonitrile (MeCN) (Figure 1A) are dominated by overlapping <sup>1</sup>ILCT and <sup>1</sup>MLCT transitions between 390 nm and 525 nm as well as a less intense feature extending up to 700 nm, which originates from direct <sup>3</sup>MLCT ← S<sub>0</sub> transitions.<sup>[57-59]</sup> The aerated complex in MeCN is weakly emissive (Φ < 0.1%) with a maximum at around 735 nm. The emission excitation spectrum reflects the absorption spectrum with the exception of a minimum at 455 nm, which falls in the range of the IP-4T ligand absorption with a band maximum at 405 nm extending to 500 nm (Figure 1A). To further rationalize this feature, resonance Raman (rR) spectra were excited at 405 and 473 nm (Figure 1B) and normalized to the MeCN band at 1374 cm<sup>-1</sup>. By comparison to the rR spectra of [Os(bpy)<sub>3</sub>]<sup>2+</sup>, **1** reveals specific bands for both bpy and IP-4T. The intensity of the bpy-related bands (e.g., at 1608 and 1556 cm<sup>-1</sup>) increased slightly upon excitation at 473 nm. However, the most prominent band is at 1452 cm<sup>-1</sup>, which is not present in the homoleptic complex. This band increased by 23% with 473 nm excitation and was assigned to the symmetrical C=C stretching mode in quaterthiophene according to the literature.<sup>[60]</sup> Together with the minimum in the emission excitation spectra at



**Scheme 1.** Molecular structures of osmium and ruthenium compounds previously investigated for PDT and Os-IP-4T (**1**) of this study. The compounds are racemic mixtures of the  $\Delta/\Lambda$  isomers.

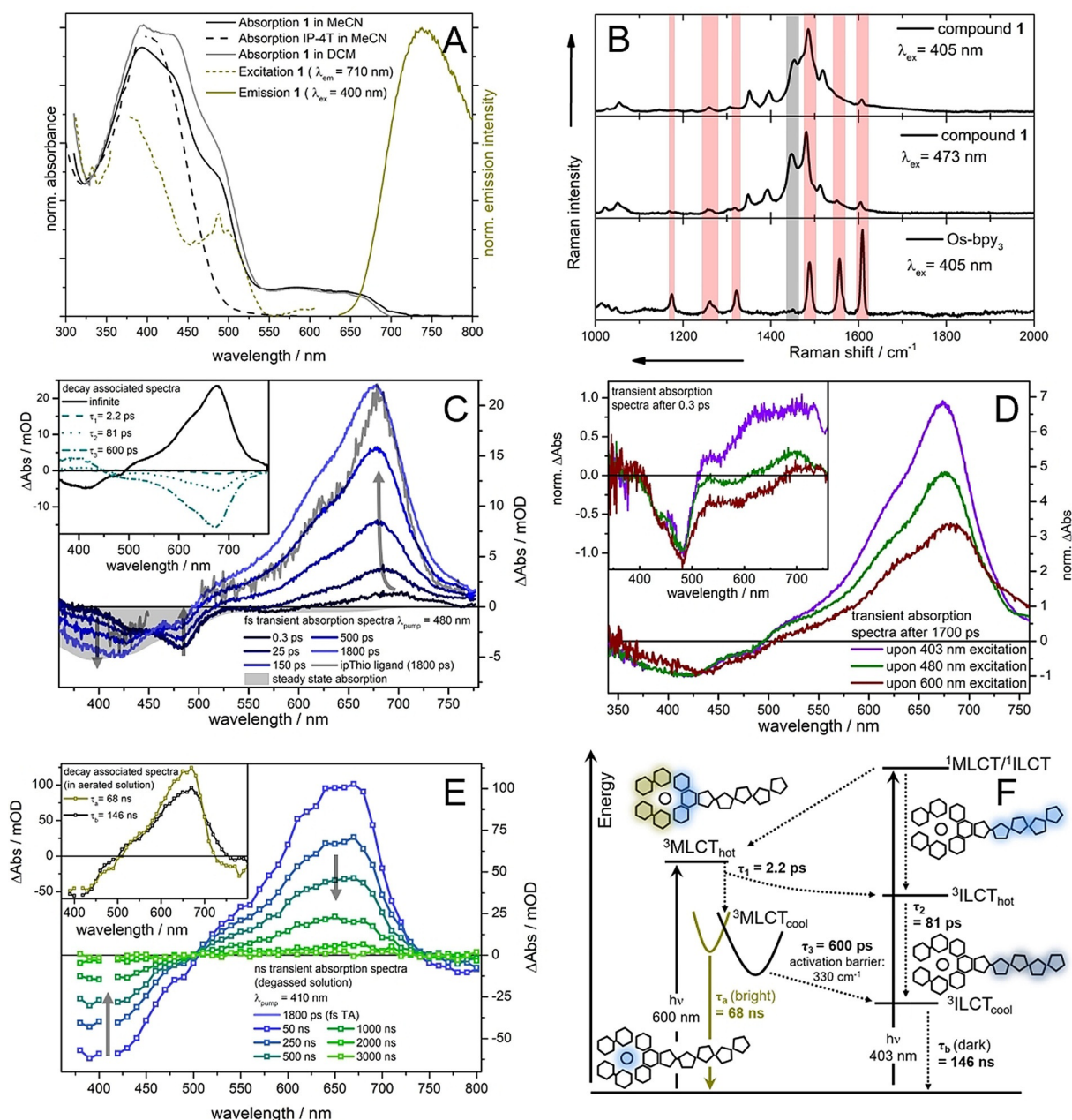


**Figure 1.** A) Steady state absorption spectra of complex 1 in DCM (grey) or ACN (black) as well as the steady state emission spectrum ( $\lambda_{\text{ex}} = 400$  nm) in ACN (dark yellow) and excitation spectrum ( $\lambda_{\text{em}} = 710$  nm) in ACN (dotted line, dark yellow). Normalized to the minimum at 325 nm (absorption and excitation) or maximum at 740 nm (emission). B) Resonance Raman (rR) spectra of 1 in ACN and  $[\text{Os}(\text{bpy})_3]^{2+}$  in water at 473 nm and 405 nm excitation. The red and grey lines indicate bpy and quaterthiophene-related Raman bands, respectively. C) Femtosecond transient absorption spectra of 1 in ACN with  $\lambda_{\text{exc}} = 480$  nm at different times, with filled and scaled steady state absorption spectrum as reference for GSB as well as the transient absorption spectrum of the free IP-4T ligand at 1800 ps in grey. As inset the respective decay associated spectra of complex 1. D) Transient absorption spectra of 1 in ACN at 1700 ps after excitation at 403 nm (violet), 480 nm (olive) and 600 nm (maroon), as inset the respective spectra at 0.3 ps delay time. Both normalized to the minimum of the GSB. E) The ns transient absorption spectra of 1 in degassed ACN solution ( $\lambda_{\text{exc}} = 410$  nm) at different times. As inset the decay associated spectra of the ns transient absorption in aerated solution. F) Proposed model of the excited state dynamics of 1. The bright deactivation pathway is depicted in yellow, while the dark is shown in black.

around 450 nm, this indicates a somewhat more prominent excitation of ILCT states, in which the excited-state transition is localized on the IP-4T ligand.

To investigate the most common mode of light-driven cytotoxicity, the capacity of 1 to generate  $^1\text{O}_2$  was examined. Monitoring the  $^1\text{O}_2$  emission in the presence of 1 and referencing against  $[\text{Ru}(\text{bpy})_3](\text{PF}_6)_2$  (in MeCN,  $\lambda_{\text{ex}} = 450$  nm) resulted in a

quantum yield for  $^1\text{O}_2$  production of 41%, which is lower than that for comparable  $\text{Ru}^{\text{II}}$  complexes, but twice as high as certain other published  $[\text{Os}(\text{bpy})_2(\text{LL})]^{2+}$  complexes.<sup>[61]</sup> The singlet-oxygen sensitization in organic solvent points to ILCT states being sufficiently long-lived for photosensitization of  $^1\text{O}_2$ . However, to understand the effect of the cellular environment and how this impacts the formation and lifetime of the triplet state

responsible for  $^1\text{O}_2$  sensitization, we first required a complete picture of the excited-state dynamics, including information on the ultrafast formation of the emissive excited state, in cell-free solution. Thus, we begin with the investigation of the photoinduced dynamics in different solvents and then present the experiments in cells.

To investigate the photoinduced dynamics outside the Franck-Condon region, femtosecond transient absorption (TA) spectra were recorded for **1** upon excitation at 480 nm (Figure 1C, see Figure 1F for the proposed model). Below 550 nm a negative signal centered at 480 nm is visible, which decays as a minimum at 420 nm develops. This negative differential absorption signal resembles the shape of the ground-state bleach (GSB) is superimposed by an excited-state absorption (ESA) signal at about 400 nm, typically observed for of  $\text{Os}^{\text{II}}$   $^3\text{MLCT}$  states,<sup>[31]</sup> which subsequently decays. We postulate that at early delay times, a triplet  $^3\text{MLCT}$ -state is present, which upon blue excitation emerges from an initial  $^1\text{MLCT}/^1\text{ILCT}$  manifold and decays with a characteristic time constant of  $\tau_3 = 600$  ps as determined via a global fit of all kinetic traces. The  $^3\text{MLCT}$ -decay does not cause decay of the GSB. Hence, the  $^3\text{MLCT}$  decay forms a secondary excited state, which is visible in the transient absorption spectra as the increasing ESA signal at 680 nm. The band at 680 nm, which emerges with  $\tau_3 = 600$  ps, correlates to the long-lived differential absorption feature of the free IP-4T ligand (Figure 1C) and agrees well with the TA signature of oligothiophenes.<sup>[62,63]</sup> Thus, we assign the long-lived species observed for **1** to an IP-4T-ligand centered  $^3\text{ILCT}$  state.<sup>[64]</sup> However, even at early delay times, the transient absorption spectrum shows a characteristic feature at 690 nm pointing to the fact that almost immediately after photoexcitation, both  $^3\text{MLCT}$  and  $^3\text{ILCT}$  states are populated.

The kinetic analysis of the transient absorption data as reflected in the decay associated spectra (DAS) shows changes in the spectral region above 600 nm at early delay times (Figure 1C). These changes can be related to the kinetic processes associated with the characteristic time constants  $\tau_1 = 2.2$  ps and  $\tau_2 = 81$  ps, i.e., on time scales where hardly any change is observed below 550 (Figure 1C).  $\tau_1 = 2.2$  ps leads to an increase of the 690 nm ESA band, likely due to a rapid partial population of the  $^3\text{ILCT}$  state from vibrationally hot  $^3\text{MLCT}$  states. This vibrationally hot  $^3\text{MLCT}$  state can also decay to the thermally relaxed  $^3\text{MLCT}_{\text{cool}}$  state through a much slower channel ( $\tau_3 = 600$  ps), which subsequently populates the geometrically relaxed  $^3\text{ILCT}_{\text{cool}}$  state (vide supra). The process associated with  $\tau_2 = 81$  ps leads to an increased ESA signal at 680 nm, which blue shifts (Figure S1 in the Supporting Information) and sharpens. A monoexponential fit of the position of the ESA maximum as a function of delay time yields a characteristic time constant of 81 ps, which is in good agreement with  $\tau_2$  as determined from a global fit. Hence,  $\tau_2$  was assigned to structural reorganization of the oligothiophene chain in the electronically excited state ( $^3\text{ILCT}_{\text{hot}} \rightarrow ^3\text{ILCT}_{\text{cool}}$ ), which could involve planarization based on fact that oligothiophenes generally adopt the more rigid and coplanar quinoidal form in the excited state.<sup>[65]</sup>

The ratio of GSB (below 500 nm) and the  $^3\text{ILCT}$ -associated ESA (between 600 and 700 nm) recorded at a delay of 0.3 ps changes as a function of excitation wavelength. Upon 600 nm excitation, where direct population of the  $^1\text{ILCT}$  state would not be expected, a transient absorption spectrum resembling the transient spectrum of  $[\text{Os}(\text{bpy})_3]^{2+}$  is observed.<sup>[31]</sup> In contrast, excitation at 403 nm causes a strong  $^3\text{ILCT}$ -associated ESA signal to become visible (Figure 1D). At long delay times, i.e., 1700 ps, a pronounced ESA signal at 690 nm associated with the reorganized  $^3\text{ILCT}_{\text{cool}}$  state is observed irrespective of the excitation wavelength. This indicates that the population initially placed into the  $^3\text{MLCT}_{\text{cool}}$  channel is transferred to the  $^3\text{ILCT}_{\text{cool}}$  state on a longer time scale. The relative growth of the  $^3\text{ILCT}_{\text{cool}}$ -associated ESA band is larger with longer excitation wavelengths and this qualitative behavior does not depend on the polarity of the solvent (Table S1). Except for a prolongation of  $\tau_1 = 4.7$  ps at 403 nm excitation, no significant changes of the characteristic time constants with excitation wavelength are observed.

To further investigate the photoinduced processes, time-resolved data were recorded as a function of temperature as well as solvent polarity (dielectric constant,  $\epsilon$ ) and viscosity ( $\mu$ ). While these variations cause changes in the rates of the respective kinetic processes, the overall picture of the transient data remains unchanged (Table S3). Increasing the viscosity of the solvent on going from MeCN ( $\epsilon = 35.7$ ;  $\mu = 0.39$  cP) to *N,N'*-dimethylpropyleneurea (DMPU) ( $\epsilon = 36.1$ ;  $\mu = 3.41$  cP) slows the overall excited-state dynamics, whereby  $\tau_2$ , associated with the structural reorganization of the thienyl rings, increases from 81 to 132 ps. The conformational flexibility of the thienyl rings of the IP-4T ligand at room temperature is hindered in the more viscous solvent, leading to a prolonged  $\tau_2$  and generally slower excited state dynamics. The prolongation of  $\tau_3$  in the more viscous DMPU suggests that the oligothiophene chain must adopt a certain geometry in order for energy transfer from the vibrationally relaxed  $^3\text{MLCT}_{\text{cool}}$  to the  $^3\text{ILCT}_{\text{cool}}$  state to occur. The energy barrier for this  $^3\text{MLCT}_{\text{cool}} \rightarrow ^3\text{ILCT}_{\text{cool}}$  transition was estimated from temperature-dependent TA experiments in MeCN (see Figure S2). The prolonged  $\tau_3$  that resulted from decreasing the temperature to 230 K yielded an energy barrier for the  $^3\text{MLCT} \rightarrow ^3\text{ILCT}_{\text{cool}}$  transition of  $4.0 \text{ kJ mol}^{-1}$  (i.e.,  $330 \text{ cm}^{-1}$ ).

This estimate for the barrier is significantly lower than the energy barrier that was estimated for interligand  $\text{MLCT}_{\text{bpy}} \rightarrow \text{MLCT}_{\text{bpy}}$  electron transfer in  $[\text{Os}(\text{bpy})_3]^{2+}$  ( $850 \text{ cm}^{-1}$ ).<sup>[66]</sup> Therefore, we assume that relaxation of the  $^3\text{MLCT}$  state via the  $^3\text{ILCT}_{\text{cool}}$  state is favored over population of the secondary bright MLCT state. Decreasing the solvent polarity from MeCN ( $\epsilon = 35.7$ ;  $\mu = 0.39$  cP) to DCM ( $\epsilon = 8.93$ ;  $\mu = 0.42$  cP), lengthened the lifetime of  $\tau_1$  from 2.2 ps in MeCN to 6.9 ps in DCM (Table S3). This rate change was analyzed in the context of Marcus-type electron transfer, whereby the  $^3\text{ILCT}_{\text{hot}}$  state is stabilized relative to the  $^3\text{MLCT}_{\text{hot}}$  state in MeCN. The driving force is larger and hence the reaction occurs with a faster rate and thus has a shorter characteristic time constant.

The excited-state dynamics were also characterized by nanosecond TA spectroscopy (Figure 1E). A global fit of the nano-

second TA data yielded two characteristic time constants, i.e.,  $\tau_a = 68$  ns and  $\tau_b = 146$  ns. The emission lifetime determined by time-correlated single-photon counting (TCSPC) measurements ( $\tau_{em} = 58$  ns) agreed with the value for  $\tau_a$  from the nanosecond TA data, and a comparison of the emission properties (Table S2) of **1** with those of  $[\text{Os}(\text{bpy})_3]^{2+}$  and the free ligand confirmed that emission from **1** was from the  $^3\text{MLCT}$  state. Therefore, the short component ( $\tau_a = 68$  ns) in the nanosecond TA experiments was assigned to the  $^3\text{MLCT}_{\text{cool}}$  state.

The  $^3\text{MLCT}$ -based emission that decays on a 60 ns timescale in concert with the 600 ps depopulation of the  $^3\text{MLCT}_{\text{cool}}$  to the  $^3\text{ILCT}_{\text{cool}}$  state suggest two different and distinct decay pathways for the  $^3\text{MLCT}_{\text{cool}}$  state. We propose a model, where two conformers in the  $^3\text{MLCT}_{\text{cool}}$  manifold exist, one of which is able to populate the  $^3\text{ILCT}_{\text{cool}}$  state, while the other is decoupled from the thiophene chain and returns radiatively to the ground state. A similar conformer-driven double potential was also seen for a pyrene-substituted Ru complex.<sup>[56]</sup> The  $^3\text{ILCT}_{\text{cool}}$  state on the other hand decays through a single pathway by intersystem crossing to the ground state with  $\tau_b = 146$  ns.

The full photophysical model is summarized in Figure 1F. Photoexcitation populates a mixture of MLCT and ILCT states, and the MLCT/ILCT ratio is determined by the excitation wavelength. Shorter excitation near 400 nm favors initial population of both  $^1\text{MLCT}$  and  $^1\text{ILCT}$  states while longer wavelength excitation near 600 nm initially populates the  $^3\text{MLCT}$  state exclusively. The vibrationally hot  $^3\text{MLCT}$  state, which is either excited directly upon 600 nm excitation or formed by very rapid intersystem crossing upon blue excitation,<sup>[66,67]</sup> partially decays into the  $^3\text{ILCT}$  state ( $\tau_1$ ). Relaxation within the  $^3\text{ILCT}$  manifold involves structural reorganization of the oligothiophene chain. This process, which is associated with  $\tau_2$ , increases electronic delocalization within the oligothiophene and causes spectroscopic shifts of the characteristic  $^3\text{ILCT}_{\text{cool}}$  absorption band at around 680 nm. The fraction of molecules remaining within the thermally relaxed  $^3\text{MLCT}$  state decays to the  $^3\text{ILCT}_{\text{cool}}$  state on a sub-ns timescale ( $\tau_3$ ) or the decoupled conformer decays radiatively ( $\tau_a$ ). The  $^3\text{ILCT}_{\text{cool}}$  on the other hand shows a dark ground-state recovery ( $\tau_b$ ).

To understand fully how **1** might act as a phototherapy agent, it is necessary to understand its photoinduced dynamics in the human cancer cells. While the localization of many photoactive transition metal complexes have been studied by luminescence microscopy in human cells,<sup>[68–71]</sup> we are not aware of any detailed investigations of the photoinduced excited-state dynamics of such photodrugs in these biological environments. To investigate the impact of the cellular environment on the photophysics, MCF7 cells were dosed with **1**, fixed and then spectroscopically interrogated. Confocal AiryScan fluorescence microscopy images after an 18 h incubation period revealed that the complex was taken up by cells and may accumulate preferentially in the cytosol and Golgi apparatus rather than the nucleus or lysosomes as it shows no enhanced co-localization with the lysosomal marker LAMP1 (Figure 2). However, more in-depth live-cell investigations would be necessary to study possible long-term lysosomal accumulation. This however is beyond the scope of this proof-of-concept study, in which

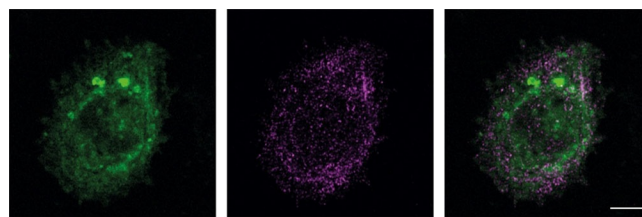


**Figure 2.** Cellular accumulation of **1**. Representative AiryScan images of MCF7 cells, incubated with **1** ( $25 \mu\text{L}^{-1}$ ) (green) for 18 h, and fixed and immunolabeled for the lysosomal marker protein LAMP1 (magenta): complex **1** (green, left), lysosomes (magenta, middle) and overlay (right). Scale bar  $5 \mu\text{m}$ .

we use fixed cells, where formalin fixation could disrupt organelle membranes and alter distribution of **1**.

Fluorescence lifetime microscopy images (FLIM) on these samples showed an average emission lifetime of 23.5 ns irrespective of the region of the cytosol interrogated (Figure S3). This lifetime agreed with the emission lifetime of **1** in aqueous solution with 3 vol% DMSO ( $\tau_{em} = 25$  ns). This indicates that the properties of the long-lived emissive  $^3\text{MLCT}$  state are not (strongly) affected by the cellular environment and fixation.

To study the ultrafast dynamics of **1** in MCF7 cells, a home-built instrument was constructed to, for the first time, record time-resolved differential absorption on fixed cells dosed with **1**. This equipment allows us to compare the photodriven response of **1** in cell-free solution with that in cells. For the transient absorption experiments, intracellular **1** was excited at 403 nm and the photoinduced dynamics were studied at various probe wavelengths in the visible range (see caption of Figure 3 for details). Based on differential optical densities recorded at individual probe wavelengths, the shape of transient absorption spectra can be estimated (Figure 3A). The estimated spectra agree well (within the range of the limited “spectral resolution”) with the transient absorption spectra recorded for **1** in cell-free solution, indicating that the overall nature of the excited states is not impacted by the local environment provided by the fixed MCF7 cells in this particular example.

The excited-state relaxation kinetics were fit to a three-exponential model. Figure 3B shows the kinetic trace recorded at 680 nm, which is modeled by a sum of exponentials yielding the characteristic time constants  $\tau_1 = 6$  ps,  $\tau_2 = 36$  ps and  $\tau_3 = 243$  ps. These characteristic time constants are in the same range as those observed for **1** in cell-free solution, further corroborating the finding that internalization of the complex into fixed cells does not impact the ultrafast dynamics qualitatively.

Cellular values for  $\tau_2$  and  $\tau_3$  are about half of the respective time-constants  $\tau_2 = 80$  ps and  $\tau_3 = 600$  ps obtained from measurements in solvents. The associated molecular processes were attributed to the structural reorganization of the oligothiophenyl group. The fact that the first-order rates associated with the structural reorganization ( $\tau_2$ ) as well as the energy transfer from the thermalized  $^3\text{MLCT}_{\text{cool}}$  to the  $^3\text{ILCT}_{\text{cool}}$  state of the reorganized oligothiophene chain ( $\tau_3$ ) are increased by a factor of roughly two indicating rigidification of the oligothiophene chain. This could be associated with intermolecular interactions between the complex and the (macro)molecular

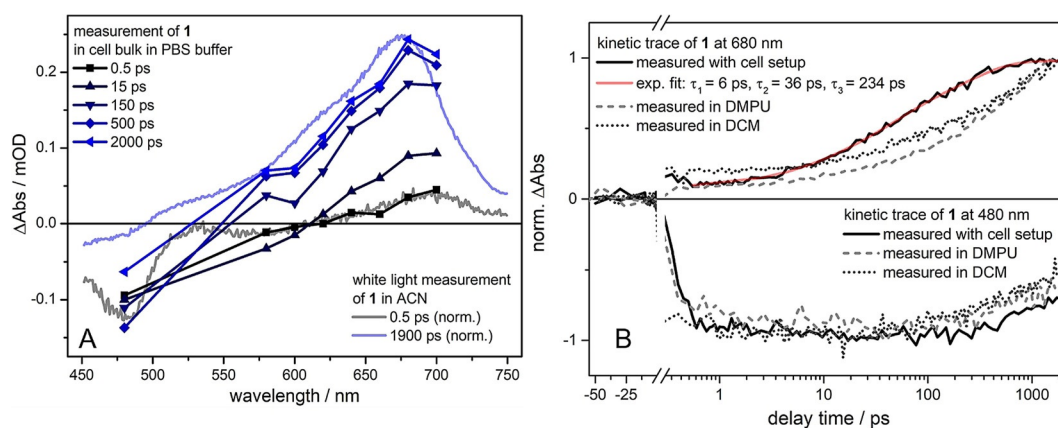


**Figure 3.** A) Femtosecond transient absorption spectra ( $\lambda_{\text{ex}} = 400$  nm) of complex **1** measured with cell setup at different times (line with symbol), probed at 480, 580, 600, 620, 640, 660, 680, and 700 nm and probed white light, measured in MeCN (normalized, solid line). B) Kinetic trace of **1** at 480 nm and 680 nm measured with cell setup (black solid line), three-exponential fit of 680 nm (red), as well as DMPU and DCM (grey, dashed, respectively dotted lines) of white light measurements.

constituents of the cells. While contributions from macromolecular cross-linking and gelation of the cytosol associated with cell fixation cannot be excluded to contribute to the effect at this stage of the study, we assume that such nonspecific fixation effects would manifest themselves similar to an increase in solvent viscosity. Nonetheless, the intracellular kinetics are very different from those measured in the highly viscous solvent, which could point to cell-specific interactions being responsible for the prolongation of  $\tau_3$ .

The intracellular ultrafast spectroscopy performed on fixed cells demonstrates proof-of-concept and is the necessary first step towards quantifying the ultrafast excited-state dynamics in living cells. These first proof-of-concept studies showed an accelerated population of the  $^3\text{ILCT}_{\text{cool}}$  state. Such an effect may prove beneficial for photoinduced toxicity since the long-lived  $^3\text{ILCT}_{\text{cool}}$  state facilitates ROS generation.<sup>[72]</sup> The excited-state dynamics observed for intracellular **1** on a sub-ns time scale and its emission suggest that specific interactions between the complex and intracellular constituents do not alter the general excited-state model for the complex, but that these interactions do have the capacity to influence the efficiency with which certain states are populated and in turn the ensuing biological properties. Thus, it is even more important to understand the photophysical dynamics inside living cells as the next step, and current efforts are underway to adapt the first-of-its-kind transient absorption setup for cell bulk measurements for making these less static, more difficult measurements.

This study presents a complete picture of the ultrafast photophysics of complex **1**, a cell-penetrating, red-light absorbing  $\text{Os}^{\text{II}}$ -based photosensitizer. With in-depth femto- and nanosecond TA measurements in a cell-free environment, we were able to ascertain that the intracellular excited-state dynamics are not significantly impacted by the biological milieu. In both cases, the photophysics are dominated by the interplay between MLCT and ILCT states.

Photoexcitation produces a mixture of  $^1\text{MLCT}/^1\text{ILCT}$  or the triplet  $^3\text{MLCT}$  states that ultimately decay to a structurally reor-

ganized longer-lived  $^3\text{ILCT}_{\text{cool}}$  state within several hundred picoseconds. Some fraction of the excited population remains in a decoupled, bright  $^3\text{MLCT}_{\text{cool}}$  state that decays radiatively. We are able to correlate the established photophysical model in solution to that in a complex cellular environment, which is the relevant environment for understanding any light-activated cytotoxicity.

The data shows that the interplay between  $^3\text{ILCT}$  states associated with the oligothiophene chain and the  $^3\text{MLCT}$  state determines the formation of long-lived excited states that are most important for ROS production. Our study revealed that the emission lifetime of the complexes in fixed MCF7 cells is uniformly distributed and is in agreement with the emission lifetime of the complex recorded in aqueous solution as well as in organic solution.

These findings and the new experimental set-up for measuring intracellular photophysics reported herein pave the way for future studies aimed at understanding how the cellular environment impacts the excited state dynamics of photosensitizers used for light-based therapies. Our future studies involve a system upgrade that will utilize microscope incubators at the sample position in order to measure living cells, thus circumventing any possible alteration of natural cell environment due to fixation. The capacity to perform intracellular photophysical studies is a prerequisite to understanding the excited-state dynamics and relating these photophysical processes to a compound's photo-triggered biological activity, which will be evaluated in systematic studies to come.

## Experimental Section

Experimental details can be found in the Supporting Information.

## Acknowledgements

K.R.A.S. thanks the Carl-Zeiss-Stiftung for support. A.C. and B.D. thank the DFG (project DI1517/18-1) for financial support. J.B.

thanks the FCI for support (Kekulé Stipendium). C.E., C.B.L. and K.R. acknowledge financial support by MRC/EPSC/BBSRC Next generation Microscopy grant (MR/K01577X/1); Wellcome Trust (Strategic Award 091911: Micron Advanced Bioimaging Unit, 203285/C/16/Z and 104924/14/Z/14.); Wolfson Foundation; MRC (MC UU 12010/unit programmes G0902418 and MC UU 12025); John Fell Fund; EPA Cephalosporin Fund; state of Thuringia (Thüringer Aufbaubank (TAB)); and the Deutsche Forschungsgemeinschaft (Research unit 1905. Jena Excellence Cluster “Balance of the Microverse” and Collaborative Research Center 1278).

We thank the Microverse Imaging Center and Aurélie Jost for providing microscope facility support for data acquisition. Open access funding enabled and organized by Projekt DEAL.

## Conflict of interest

The authors declare no conflict of interest.

**Keywords:** in vitro spectroscopy · oligothiophene · osmium polypyridyl · transient absorption · ultrafast spectroscopy

- [1] A. Levina, A. Mitra, P. A. Lay, *Metalomics* **2009**, *1*, 458–470.
- [2] H. A. Wee, P. J. Dyson, *Eur. J. Inorg. Chem.* **2006**, 4003–4018.
- [3] C. Mari, V. Pierroz, S. Ferrari, G. Gasser, *Chem. Sci.* **2015**, *6*, 2660–2686.
- [4] T. J. Dougherty, C. J. Gomer, B. W. Henderson, G. Jori, D. Kessel, M. Korbelik, J. Moan, Q. Peng, *J. Natl. Cancer Inst.* **1998**, *90*, 889–905.
- [5] I. J. MacDonald, T. J. Dougherty, *J. Porphyrins Phthalocyanines* **2001**, *05*, 105–129.
- [6] F. Caruso, M. Rossi, A. Benson, C. Opazo, D. Freedman, E. Monti, M. B. Gariboldi, J. Shaulky, F. Marchetti, R. Pettinari, C. Pettinari, *J. Med. Chem.* **2012**, *55*, 1072–1081.
- [7] D. E. J. G. Dolmans, D. Fukumura, R. K. Jain, *Nat. Rev. Cancer* **2003**, *3*, 380–389.
- [8] N. J. Farrer, P. J. Sadler, *Aust. J. Chem.* **2008**, *61*, 669–674.
- [9] N. J. Farrer, L. Salassa, P. J. Sadler, *Dalton Trans.* **2009**, *48*, 10660–10669.
- [10] L. Zeng, P. Gupta, Y. Chen, E. Wang, L. Ji, H. Chao, Z. S. Chen, *Chem. Soc. Rev.* **2017**, *46*, 5771–5804.
- [11] J. D. Knoll, C. Turro, *Coord. Chem. Rev.* **2015**, *282–283*, 110–126.
- [12] S. Bonnet, *Dalton Trans.* **2018**, *47*, 10330–10343.
- [13] J. M. Fernandez, M. D. Bilgin, L. I. Grossweiner, *J. Photochem. Photobiol. B* **1997**, *37*, 131–140.
- [14] M. Ochsner, *J. Photochem. Photobiol. B* **1997**, *39*, 1–18.
- [15] K. Plaetzer, B. Krammer, J. Berlanda, F. Berr, T. Kiesslich, *Lasers Med. Sci.* **2009**, *24*, 259–268.
- [16] B. S. Howerton, D. K. Heidary, E. C. Glazer, *J. Am. Chem. Soc.* **2012**, *134*, 8324–8327.
- [17] E. Wachter, D. K. Heidary, B. S. Howerton, S. Parkin, E. C. Glazer, *Chem. Commun.* **2012**, *48*, 9649–9651.
- [18] E. Wachter, B. S. Howerton, E. C. Hall, S. Parkin, E. C. Glazer, *Chem. Commun.* **2014**, *50*, 311–313.
- [19] T. Sainuddin, M. Pinto, H. Yin, M. Hetu, J. Colpitts, S. A. McFarland, *J. Inorg. Biochem.* **2016**, *158*, 45–54.
- [20] J. Roque, D. Havrylyuk, P. C. Barrett, T. Sainuddin, J. McCain, K. Colón, W. T. Sparks, E. Bradner, S. Monro, D. Heidary, C. G. Cameron, E. C. Glazer, S. A. McFarland, *Photochem. Photobiol.* **2020**, *96*, 327–339.
- [21] L. M. Loftus, J. K. White, B. A. Albani, L. Kohler, J. J. Kodanko, R. P. Thummel, K. R. Dunbar, C. Turro, *Chem. Eur. J.* **2016**, *22*, 3704–3708.
- [22] K. Arora, M. Herroon, M. H. Al-Afyouni, N. P. Toupin, T. N. Rohrabough, L. M. Loftus, I. Podgorski, C. Turro, J. J. Kodanko, *J. Am. Chem. Soc.* **2018**, *140*, 14367–14380.
- [23] L. N. Lameijer, D. Ernst, S. L. Hopkins, M. S. Meijer, S. H. C. Askes, S. E. Le Dévédec, S. Bonnet, *Angew. Chem. Int. Ed.* **2017**, *56*, 11549–11553; *Angew. Chem.* **2017**, *129*, 11707–11711.
- [24] J. A. Cuello-Garibo, C. C. James, M. A. Siegler, S. L. Hopkins, S. Bonnet, *Chem. Eur. J.* **2019**, *25*, 1260–1268.
- [25] J.-A. Cuello-Garibo, C. C. James, M. A. Siegler, S. Bonnet, *Chem. Squared* **2017**, *1*, 1–19.
- [26] J.-P. Collin, S. Guillerez, J.-P. Sauvage, F. Barigelletti, L. Flamigni, L. De Cola, V. Balzani, *Coord. Chem. Rev.* **1991**, *111*, 291–296.
- [27] P. C. A. Bruijninx, P. J. Sadler, *Controlling Platinum, Ruthenium, and Osmium Reactivity for Anticancer Drug Design*, Elsevier, **2009**.
- [28] Y. Fu, M. J. Romero, A. Habtemariam, M. E. Snowden, L. Song, G. J. Clarkson, B. Qamar, A. M. Pizarro, P. R. Unwin, P. J. Sadler, *Chem. Sci.* **2012**, *3*, 2485–2494.
- [29] I. Romero-Canelón, L. Salassa, P. J. Sadler, *J. Med. Chem.* **2013**, *56*, 1291–1300.
- [30] A. Bergamo, A. Masi, A. F. A. Peacock, A. Habtemariam, P. J. Sadler, G. Sava, *J. Inorg. Biochem.* **2010**, *104*, 79–86.
- [31] Y. Sun, L. E. Joyce, N. M. Dickson, C. Turro, *Chem. Commun. (Camb.)* **2010**, *46*, 6759–6761.
- [32] R. J. Needham, C. Sanchez-Cano, X. Zhang, I. Romero-Canelón, A. Habtemariam, M. S. Cooper, L. Meszaros, G. J. Clarkson, P. J. Blower, P. J. Sadler, *Angew. Chem. Int. Ed.* **2017**, *56*, 1017–1020; *Angew. Chem.* **2017**, *129*, 1037–1040.
- [33] Y. Fu, A. Habtemariam, A. M. B. H. Basri, D. Braddick, G. J. Clarkson, P. J. Sadler, *Dalton Trans.* **2011**, *40*, 10553.
- [34] M. Hanif, M. V. Babak, C. G. Hartinger, *Drug Discovery Today* **2014**, *19*, 1640–1648.
- [35] Y. Fu, A. Habtemariam, A. M. Pizarro, S. H. Van Rijt, D. J. Healey, P. A. Cooper, S. D. Shnyder, G. J. Clarkson, P. J. Sadler, *J. Med. Chem.* **2010**, *53*, 8192–8196.
- [36] S. H. Van Rijt, A. Mukherjee, A. M. Pizarro, P. J. Sadler, *J. Med. Chem.* **2010**, *53*, 840–849.
- [37] A. F. A. Peacock, S. Parsons, P. J. Sadler, *J. Am. Chem. Soc.* **2007**, *129*, 3348–3357.
- [38] S. H. Van Rijt, I. Romero-Canelón, Y. Fu, S. D. Shnyder, P. J. Sadler, *Metalomics* **2014**, *6*, 1014–1022.
- [39] Y. Fu, R. Soni, M. J. Romero, A. M. Pizarro, L. Salassa, G. J. Clarkson, J. M. Hearn, A. Habtemariam, M. Wills, P. J. Sadler, *Chem. Eur. J.* **2013**, *19*, 15199–15209.
- [40] S. H. Van Rijt, H. Kostrhunova, V. Brabec, P. J. Sadler, *Bioconjugate Chem.* **2011**, *22*, 218–226.
- [41] S. D. Shnyder, Y. Fu, A. Habtemariam, S. H. Van Rijt, P. A. Cooper, P. M. Loadman, P. J. Sadler, *Med. Chem. Comm.* **2011**, *2*, 666–668.
- [42] A. Byrne, C. Dolan, R. D. Moriarty, A. Martin, U. Neugebauer, R. J. Forster, A. Davies, Y. Volkov, T. E. Keyes, *Dalton Trans.* **2015**, *44*, 14323–14332.
- [43] P. Zhang, H. Huang, *Dalton Trans.* **2018**, *47*, 14841–14854.
- [44] S. A. E. Omar, P. A. Scattergood, L. K. McKenzie, C. Jones, N. J. Patmore, A. J. H. M. Meijer, J. A. Weinstein, C. R. Rice, H. E. Bryant, P. I. P. Elliott, *Inorg. Chem.* **2018**, *57*, 13201–13212.
- [45] P. Zhang, Y. Wang, K. Qiu, Z. Zhao, R. Hu, C. He, Q. Zhang, H. Chao, *Chem. Commun.* **2017**, *53*, 12341–12344.
- [46] S. Omar, P. Scattergood, L. McKenzie, H. Bryant, J. Weinstein, P. Elliott, *Molecules* **2016**, *21*, 1382.
- [47] C. Ge, H. Huang, Y. Wang, H. Zhao, P. Zhang, Q. Zhang, *ACS Appl. Biol. Mater.* **2018**, *1*, 1587–1593.
- [48] S. Lazic, P. Kaspler, G. Shi, S. Monro, T. Sainuddin, S. Forward, K. Kasimova, R. Hennigar, A. Mandel, S. McFarland, L. Lilge, *Photochem. Photobiol.* **2017**, *93*, 1248–1258.
- [49] R. S. Lumpkin, E. M. Kober, L. A. Worl, Z. Murtaza, T. J. Meyer, *J. Phys. Chem.* **1990**, *94*, 239–243.
- [50] P. A. Scattergood, D. A. W. Ross, C. R. Rice, P. I. P. Elliott, *Angew. Chem. Int. Ed.* **2016**, *55*, 10697–10701; *Angew. Chem.* **2016**, *128*, 10855–10859.
- [51] E. C. Glazer, *Photochem. Photobiol.* **2017**, *93*, 1326–1328.
- [52] Y. Arenas, S. Monro, G. Shi, A. Mandel, S. McFarland, L. Lilge, *Photodiagn. Photodyn. Ther.* **2013**, *10*, 615–625.
- [53] J. Fong, K. Kasimova, Y. Arenas, P. Kaspler, S. Lazic, A. Mandel, L. Lilge, *Photochem. Photobiol. Sci.* **2015**, *14*, 2014–2023.
- [54] G. Shi, S. Monro, R. Hennigar, J. Colpitts, J. Fong, K. Kasimova, H. Yin, R. DeCoste, C. Spencer, L. Chamberlain, et al., *Coord. Chem. Rev.* **2015**, *282–283*, 127–138.
- [55] S. Monro, K. L. Colón, H. Yin, J. Roque, P. Konda, S. Gujar, R. P. Thummel, L. Lilge, C. G. Cameron, S. A. McFarland, *Chem. Rev.* **2019**, *119*, 797–828.

- [56] C. Reichardt, T. Sainuddin, M. Wächtler, S. Monro, S. Kupfer, J. Guthmüller, S. Gräfe, S. McFarland, B. Dietzek, *J. Phys. Chem. A* **2016**, *120*, 6379–6388.
- [57] E. Ronca, F. De Angelis, S. Fantacci, *J. Phys. Chem. C* **2014**, *118*, 17067–17078.
- [58] R. Siebert, A. Winter, U. S. Schubert, M. Schmitt, B. Dietzek, J. Popp, *Proc. SPIE* **7722**, **2010**, 77221U.
- [59] S. Decurtins, F. Felix, J. Ferguson, H. U. Guedel, A. Ludi, *J. Am. Chem. Soc.* **1980**, *102*, 4102–4106.
- [60] P. M. Viruela, R. Viruela, E. Ortí, J. Casado, V. Hernández, J. T. López Navarrete, *J. Mol. Struct.* **2003**, 651–653, 657–664.
- [61] A. A. Abdel-Shafi, D. R. Worrall, A. Y. Ershov, *Dalton Trans.* **2004**, 30–36.
- [62] D. Grebner, M. Helbig, S. Rentsch, *J. Phys. Chem.* **1995**, *99*, 16991–16998.
- [63] S. Rentsch, J. P. Yang, W. Paa, E. Birckner, J. Schiedt, R. Weinkauff, *Phys. Chem. Chem. Phys.* **1999**, *1*, 1707–1714.
- [64] Private Communication of Unpublished Results with Sherri McFarland and Coworkers, **2020**.
- [65] J. P. Yang, W. Paa, S. Rentsch, *Chem. Phys. Lett.* **2000**, *320*, 665–672.
- [66] G. B. Shaw, D. J. Styers-Barnett, E. Z. Gannon, J. C. Granger, J. M. Papanikolas, *J. Phys. Chem. A* **2004**, *108*, 4998–5006.
- [67] O. Bräm, F. Messina, E. Baranoff, A. Cannizzo, M. K. Nazeeruddin, M. Chergui, *J. Phys. Chem. C* **2013**, *117*, 15958–15966.
- [68] V. Fernández-Moreira, F. L. Thorp-Greenwood, M. P. Coogan, *Chem. Commun.* **2010**, 46, 186–202.
- [69] D. L. Ma, H. Z. He, K. H. Leung, D. S. H. Chan, C. H. Leung, *Angew. Chem. Int. Ed.* **2013**, *52*, 7666–7682; *Angew. Chem.* **2013**, *125*, 7820–7837.
- [70] K. K. W. Lo, S. P. Y. Li, *RSC Adv.* **2014**, *4*, 10560–10585.
- [71] M. P. Coogan, V. Fernández-Moreira, *Chem. Commun.* **2014**, *50*, 384–399.
- [72] C. Reichardt, S. Monro, F. H. Sobotta, K. L. Colón, T. Sainuddin, M. Stephenson, E. Sampson, J. Roque, H. Yin, J. C. Brendel, C. G. Cameron, S. McFarland, B. Dietzek, *Inorg. Chem.* **2019**, *58*, 3156–3166.

---

Manuscript received: June 2, 2020

Revised manuscript received: July 26, 2020

Accepted manuscript online: August 6, 2020

Version of record online: October 14, 2020